ACS APPLIED MATERIALS & INTERFACES

Research Article

www.acsami.org

Chemical Bonding-Induced Low Dielectric Loss and Low Conductivity in High-K Poly(vinylidenefluoride-trifluorethylene)/Graphene Nanosheets Nanocomposites

Fei Wen,[†,‡] Zhuo Xu,[‡] Shaobo Tan,[†] Weimin Xia,[‡] Xiaoyong Wei,[‡] and Zhicheng Zhang*[,†]

[†]Department of Applied Chemistry, MOE Key Laboratory for Nonequilibrium Synthesis and Modulation of Condensed Matter, School of Science, Xi'an Jiaotong University, Xi'an 710049, P. R. China

[‡]Electronic Materials Research Laboratory, Key Laboratory of the Ministry of Education & International Center for Dielectric Research, Xi'an Jiaotong University, Xi'an 710049, P. R. China

ABSTRACT: Blending high-permittivity (ε_r) ceramic powders or conductive fillers into polymers to form 0-3-type composites has been regarded as one of the most promising processes to achieve high-dielectric-permittivity materials with excellent processing performance. The high dielectric loss and conductivity induced by the interface between the matrix and fillers as well as the leakage current have long been a great challenge of dielectric composites, and the resolution of these challenges is still an open question. In this work, poly(vinylidenefluoride-trifluorethylene with double bonds)/graphene nanosheets (P(VDF-TrFE-DB)/GNS) terpolymer nanocomposites were fabricated via a solution-cast process. GNSs were functionalized with KH550 to improve the dispersion in the terpolymer matrix solution and crosslinked with P(VDF-TrFE-DB) by a free-radical addition reaction in the nanocomposites. Compared with neat terpolymer, significantly increased dielectric permittivity and a low loss were observed for the composites. For instance, at 1 kHz the P(VDF-TrFE-DB)/GNS composites with 4 vol % GNS possessed a dielectric permittivity of 74, which is over seven times larger than that of neat terpolymer. However, a rather low dielectric loss (0.08 at 1 kHz) and conductivity (3.47×10^{-7} S/m at 1 kHz) are observed in the P(VDF-TrFE-DB)/GNS composites containing up to 12 vol % GNS. The covalent bonding constructed between P(VDF-TrFE-DB) and GNS is responsible for the reduced aspect ratio of the GNS and the crystalline properties of P(VDF-TrFE-DB) as well as the improved compatibility between them. As a result, the high-dielectric-loss conductivity of polymer composites, mainly induced by conduction loss and the interface polarization between the matrix and filler, were effectively restricted. Meanwhile, the 3D network established between P(VDF-TrFE-DB) and GNS endows the P(VDF-TrFE-DB)/GNS composites at high temperature with excellent mechanical and dielectric properties. Besides preparing high-performance dielectric composites, this facile route may also be utilized to fabricate high-performance nanocomposites by inhibiting the poor compatibility between fillers and polymeric matrix.

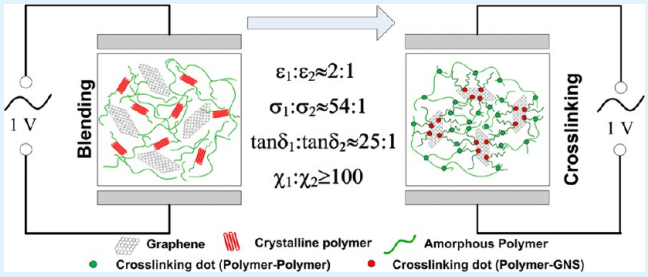

KEYWORDS: *P(VDF-TrFE), GNS, dielectric permittivity, low dielectric loss*

1. INTRODUCTION

Poly(vinylidene fluoride) (PVDF)-based ferroelectric polymers, such as poly(vinylidenefluoride-co-trifluorethylene) (P(VDF-TrFE)) and poly(vinylidenefluoride-co-trifluorethylene-co-chlorotrifluoroethylene) (P(VDF-TrFE-CTFE)), have attracted considerable attention for applications in microelectromechanical devices and high-charge storage capacitors over the past decades.[1−6] Dispersing high-permittivity (ε_r) ceramic powders (e.g., BT, PT, PZT, CCTO, etc.) into these polymers to form 0-3-type composites has been regarded as one of the most promising processes to enhance their ε_r further. Nevertheless, at high particulate loading, which was necessary for achieving high ε_r, ceramic-loaded composites lose their flexibility undesirably.[7−11] To overcome the limitations of ceramic-loaded composites, many promising works have been carried out recently on the basis of percolation theory. Namely, a small volume fraction of conductive fillers was added to the polymer matrix to achieve a high ε_r value at the percolation threshold of the composites while preserving the mechanical flexibility of the polymer.[7−11]

Among the numerous conductive fillers reported, carbon-based materials have been investigated mostly for their low density, fine miscibility with polymeric matrix, and high conductivity. For instance, Dang et al. reported a PVDF/carbon-nanotubes (CNTs) composite with a percolation threshold of 8 vol % that possesses an ε_r of 600 and a dielectric loss (tan δ) of about 2 at 1 kHz at a CNTs loading content of 8 vol %.[9] The percolation threshold of these

Received: May 13, 2013
Accepted: September 9, 2013
Published: September 9, 2013

   dx.doi.org/10.1021/am401784p | *ACS Appl. Mater. Interfaces* 2013, 5, 9411−9420

composites is known to be strongly dependant on the filler morphology, and conductive particles with a large aspect ratio have a relatively low threshold for the easily achieved direct contact between filler particles.[12] Recently, graphene nanosheets (GNS) have been widely investigated in the polymer nanocomposite field for their high surface-to-volume ratio and high electric conductivity.[13−19] Blending a low loading content GNS into PVDF-based ferroelectric polymers could improve ε_r of the polymer matrix dramatically because of the low percolation threshold and high aspect ratio of GNS.[20−28] For instance, PVDF/GNS composites reported by Tang et al. had an ε_r value of 650 at a GNS loading content of 2.7 vol %.[20] However, a large dielectric loss is usually observed at the high ε_r composition of these composites, which is mainly induced by the leakage current among the conductive fillers at their threshold content. The adverse agglomeration of GNS has been addressed as one of the reasons for the high loss and conductivity in these composites. Therefore, many efforts have been made to enhance the dispersion uniformity of GNS in a polymer matrix by surface-modifying the GNS chemically. Although the dispersion of the GNS in polymer matrix could improve the characteristics because of better dispersion into organic solvent as well as elevated mechanical properties of the composites, limited success has been achieved in reducing the dielectric loss and conductivity in the composites with high ε_r. Meanwhile, it is always risky to use percolative dielectrics at their threshold composition because of the abrupt variations of ε_r, tan δ, and the conductivity near the threshold. Therefore, the ability to maintain the low dielectric loss and low conductivity in the high dielectric PVDF/GNS composites over a wide composition range is a great challenge for scientists and is still an open question so far.

Following the percolation theory, the high conductivity at threshold of these composites is mainly induced by the connectivity of the conductive fillers in the composites. With the higher the aspect ratio of the fillers, a lower threshold and higher dielectric loss induced by the leakage current would be achieved. Unfortunately, the GNS synthesized from the current widely applied synthesis process from the reduction of graphite oxide usually prossesses a high aspect ratio for the particle-size limitation of graphite. It has been well recognized that the excellent conductive properties of GNS are derived from its perfectly constructed in-plane π-conjugated structure on a large scale, and any defect introduced into the π-conjugated structure would lead to the conductivity reduction of the whole sheet. Therefore, we would like to present a chemical method to tailor the effective aspect ratio of GNS via an in situ radical addition reaction between the polymer matrix and GNS in this work. In this process, unsaturated P(VDF-TrFE), named P(VDF-TrFE-DB), is blended with surface-modified GNS together with benzyl peroxide (BPO) as a free-radical initiator in solution. At elevated temperature, the free radicals generated from the decomposition of BPO would add to the double-bonds on the P(VDF-TrFE-DB) chain. The radical addition reaction would happen between the macro free radicals formed on the polymer backbone and double-bonds on GNS subsequently. The chemical bonds formed between the P(VDF-TrFE-DB) matrix and GNS are expected to improve their compatibility and reduce the dielectric loss induced by the interface between them. The defect induced by the addition reaction from the polymeric radicals onto GNS is responsible for the enhanced threshold composition and the reduced dielectric loss and conductivity of the resultant composites even at a relatively high GNS loading content.

2. EXPERIMENTAL SECTION

2.1. Materials. GNS (graphene nanosheets) was prepared by a three-step process as follows.[29] Graphite oxide (GO) was prepared first through the oxidation of graphite powder following the modified Hummers method. GNS was synthesized by reducing GO with H_2 at 800 °C for 1 h, where GO was thermally expanded in a 50 ml Teflon-lined autoclave for 1 h at 250 °C before use. γ-Aminopropyl triethoxysilane (KH550, AR grade) and benzoyl peroxide (BPO, AR grade) were purchased from Aldrich and used as received. Ethyl alcohol (Xi'an Reagents Co. Ltd, AR grade) and *N*,*N*-dimethylformamide (DMF, Tianjin Reagents Co. Ltd, AR grade) were used as received. P(VDF-co-CTFE) (80/20) with 20 mol % CTFE was purchased from Solvay Solexis.

2.2. Synthesis of P(VDF-TrFE-CTFE) via a Hydrogenation Process of P(VDF-CTFE). The hydrogenation of P(VDF-CTFE) was conducted following a procedure reported in the literature.[30] To a 500 mL three-necked flask were added P(VDF-CTFE) copolymer (CTFE 20 mol %, 10.0 g) and AIBN (0.39 g, 2.38 mmol), and the flask was purged under vacuum with nitrogen three times before purified THF (200 mL) was injected. Stirring for 30 min at 60 °C resulted in a homogeneous solution. Then nBu_3SnH (6.5 mL, 23.8 mmol) was injected into the mixture by syringe. The reaction was carried out at 60 °C for 24 h before it was quenched with methanol. The reaction mixture was precipitated in a 1:1 v/v methanol/water mixture and washed with *n*-hexane. The crude product was redissolved in acetone and precipitated in 1:1 methanol/water three times. Finally, the product was dried in a vacuum oven at room temperature. The chemical composition of the resultant copolymer was determined to be VDF/TrFE/CTFE = 80/18/2 mol % by ^{1}H NMR.

2.3. Synthesis of the P(VDF-TrFE) Copolymer Containing Internal Double Bonds via a Dehydrochlorination Process. The dehydrochlorination reaction of P(VDF-TrFE-CTFE) was performed as in a previous report.[31] To a 250 mL two-necked flask equipped with a condenser and a magnetic stirrer were added P(VDF-TrFE-CTFE) terpolymer (5.0 g), triethylamine (3 mL, 21.4 mmol), and NMP (100 mL). The temperature was maintained at 50 °C for 24 h once the polymer was dissolved. The resultant mixture was precipitated in about 5 vol % hydrochloric acid to remove the residual TEA. The resultant copolymer was dissolved in acetone followed by precipitating in methanol three times and drying at room temperature under reduced pressure. ^{1}H and ^{19}F NMR were used to determine the exact composition of the resultant copolymers.

2.4. Preparation of the P(VDF-TrFE-DB)/GNS Composites via a Free-Radical Addition Reaction. The surface modification of GNS with KH550 was facilely conducted by dispersing GNS (0.1 g) into a KH550 ethyl alcohol solution (5 vol %, 20 mL) with stirring and sonication for 2 h at ambient temperature followed by washing the solid thoroughly with ethyl alcohol and drying it for 12 h under reduced pressure at 40 °C.

Benzoyl peroxide (BPO, 5 wt %) as an initiator was added into the P(VDF-TrFE-DB) solution (3 g/100 mL) in dimethylformamide (DMF) followed by dispersing KH550−modified GNS particles into the obtained solution. The suspension was stirred vigorously for 4 h. The films were fabricated via casting the P(VDF-TrFE-DB)/GNS suspension onto quartz slides followed by evaporating the solvent completely at 100 °C under reduced pressure. The films were then cured at 200 °C for 8 h followed by immediate quenching in an ice-water bath (0 °C). A series of P(VDF-TrFE-DB)/GNS composites containing different volume fractions (f) of grapheme nanosheets (1, 2, 4, 6, 8, and 12%) were fabricated with a thickness ranging from 24 to 30 μm. Moreover, 4% fractions of modified GNS-loaded composites of P(VDF-TrFE-CTFE)/GNS were fabricated and tested under the same conditions for comparison.

2.5. Characterization. ^{1}H and ^{19}F NMR spectra were measured on a Bruker (Advance III) 400 MHz spectrometer with acetone-d_6 as the solvent and tetramethylsilane as an internal standard. The microstructures of the composites were investigated by transmission

electron microscopy (TEM) performed on a JEOL JEM-3010 at 200 kV and a field-emission gun scanning electron microscopy (JEOL JSM6700 F). Raman scattering was measured at room temperature using Nicolet, ALMEGSA, with an excitation wavelength of 523 nm. Fourier transform infrared (FTIR) spectroscopic measurements were made with an IR spectrophotometer (Bruker-Tensor 27). X-ray photoelectron spectra (XPS) measurements were performed using a Kratos AXIS Ultra DLD system (Shimadzu Co., Ltd.) equipped with a hemispherical electron analyzer and a scanning monochromatic Al Kα (υ = 1486.6 eV) X-ray source. The thermal transition data were obtained with a TA Instruments Q100 differential scanning calorimeter (DSC) at a heating rate of 10 °C/min. For electric characterizations, gold electrodes (thickness, 80 nm; diameter, 2 mm) were sputtered on both surfaces of the films by the JEOL JFC-1600 auto fine coater. The dielectric properties were characterized at different frequencies and temperatures using an HP4294A LCR meter.

3. RESULTS AND DISCUSSION

3.1. Synthesis and Characterization of P(VDF-TrFE-DB). The precursor polymer, P(VDF-TrFE-CTFE) terpolymers, was prepared by the partial hydrogenation of P(VDF-co-CTFE) containing 20 mol % CTFE. The structure and composition of the resultant copolymers were characterized with ^{1}H NMR, as shown in Figure 1a. The two peaks appearing at 2.2−2.7 and 2.7−3.2 ppm in the original P(VDF-CTFE) are well-known head−head (−CF_2−CH_2−CH_2−CF_2−) and head−tail (−CF_2−CH_2−CF_2−CH_2−) connections of VDF units. The peak at 5.1−5.9 ppm is identified as the protons on the TrFE (−CF*H*−CF_2−) unit converted from CTFE in the terpolymer. Compared with the ^{1}H NMR spectra of P(VDF-TrFE-CTFE), new multiple peaks emerging at 6.2−6.9 ppm in the unsaturated P(VDF-TrFE) are assigned to the protons on the double bonds (−CF_2−CF=C*H*−CF_2−) after the removal of HCl from (−CF_2−CF*Cl*−CH_2−CF_2−).

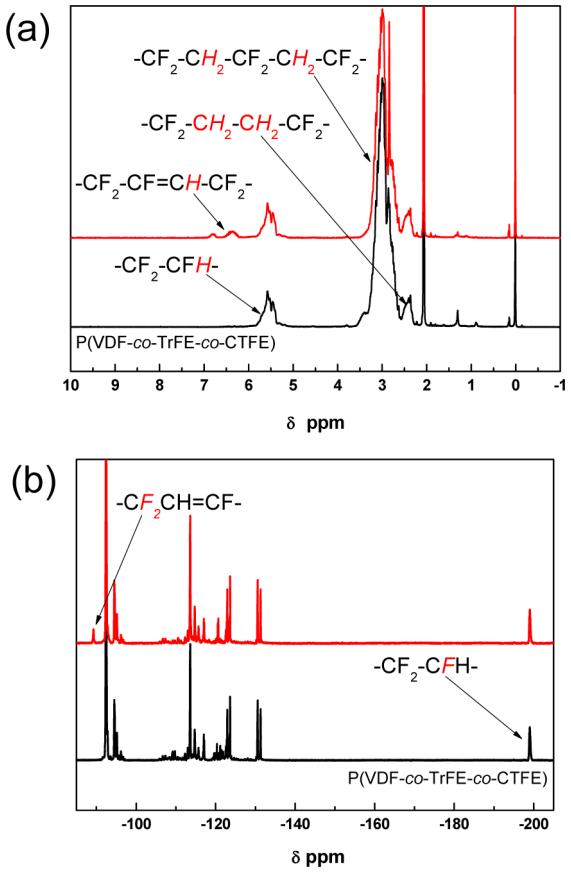

Figure 1. (a) ^{1}H NMR and (b) ^{19}F NMR spectra of P(VDF-TrFE-CTFE) (VDF/TrFE/CTFE 80/18/2 mol %) and P(VDF-TrFE-DB) (VDF/TrFE/DB 80/18/2 mol %).

The unsaturated P(VDF-TrFE) could also be confirmed by ^{19}F NMR, as shown in Figure 1b. The structure of P(VDF-co-CTFE) is dominated by the presence of a VDF−VDF head−tail (−CH_2−CF_2−CH_2−CF_2−) sequence appearing around −92.7 ppm and a VDF-CTFE tail−tail (−CF_2−CH_2−CCl*F*−CF_2−) structure appearing around −94.0, −109.1, −120.3, and −121.5 ppm. The main structure of the P(VDF-TrFE-CTFE) terpolymer includes a VDF−VDF head−tail sequence, VDF−CTFE tail−tail sequence, and VDF−TrFE tail−tail (−CF_2−CH_2−CH*F*−CF_2−) structure appearing around −199.2 ppm. Compared with the terpolymer, the new signal emerging at −89.2 ppm in unsaturated P(VDF-TrFE) could be identified as the F atoms in the double bond (−CF_2CH=C*F*−CF_2−) units.

3.2. Characterization of GNS and P(VDF-TrFE-DB)/GNS Composites. The structure of GNS was confirmed with XPS spectra and SEM and TEM images, as shown in Figure 2. Four binding energy peaks of C 1s for GNS and the hybrid are obtained by multiple-peaks fitting (inset in Figure 2a). The binding-energy peaks of GNS at 284.6, 285.6, and 290.7 eV are attributed to the nonoxygenated carbon component of C=C (sp^2), C−C (sp^3), and π−π^*, respectively, whereas the broad weak peak at 287.5 eV is assigned to oxygenated carbon component C−O−C.[32−35] GNSs were composed of randomly aggregated, thin, and wrinkled sheets loosely associated with each other, as suggested by SEM (Figure 2b) and TEM (Figure 2c).[20−22] The stacking sheet structure and individual monolayer of GNS could be observed from the high-magnification TEM image (Figure 2d). The selected-area electron diffraction (SAED) pattern of GNS (inset in Figure 2d) yielded a circular pattern, as expected for a multilayer graphene sheets. The average lateral dimensions of the GNS were on the order of 400 nm, indicating a high aspect ratio.

GNS were successfully modified with KH550 and confirmed by comparing the FTIR spectra of pure GNS, KH550, and KH550−modified GNS in Figure 3. Characteristic peaks of GNS, including 1580 cm^{-1}, corresponding to C=C of the conjugated network of aromatic groups with sp^2 hybridization, and 1260 cm^{-1}, corresponding to cyclic ether moieties such as furan or pyran,[20,35−38] were both broadened in KH550−modified GNS, which indicates that KH550 has been chemically anchored onto GNS.

The chemical structures of GNS in P(VDF-TrFE-DB)/GNS composites were investigated with Raman spectra, as shown in Figure 4, where Raman spectra of the two composites samples together with GNS filler were determined with 524 nm laser excitation. The absorption bands observed at 1584 and 1350 cm^{-1} on the Raman spectrum were attributed to the G (the E_{2g} phonon mode of sp^2 carbon atoms) and D (the breathing mode of k-point mode of A_{1g} symmetry) bands for GNS, respectively.[32,39] It has been well established that both the G and D bands undergo significant changes upon the amorphization of graphite because amorphous carbon contains a certain fraction of sp^3 carbons.[39] I_D/I_G (the intensity ratio of the D band relative to the G band) is widely utilized to measure the degree of disorder and the average size of the sp^2 domains.[39,40] The I_D/I_G ratio is increased from 0.84 for GNS fillers to 0.94 for P(VDF-TrFE-DB)/GNS, corresponding to a 11.9% increment compared to neat GNS, whereas a negligible

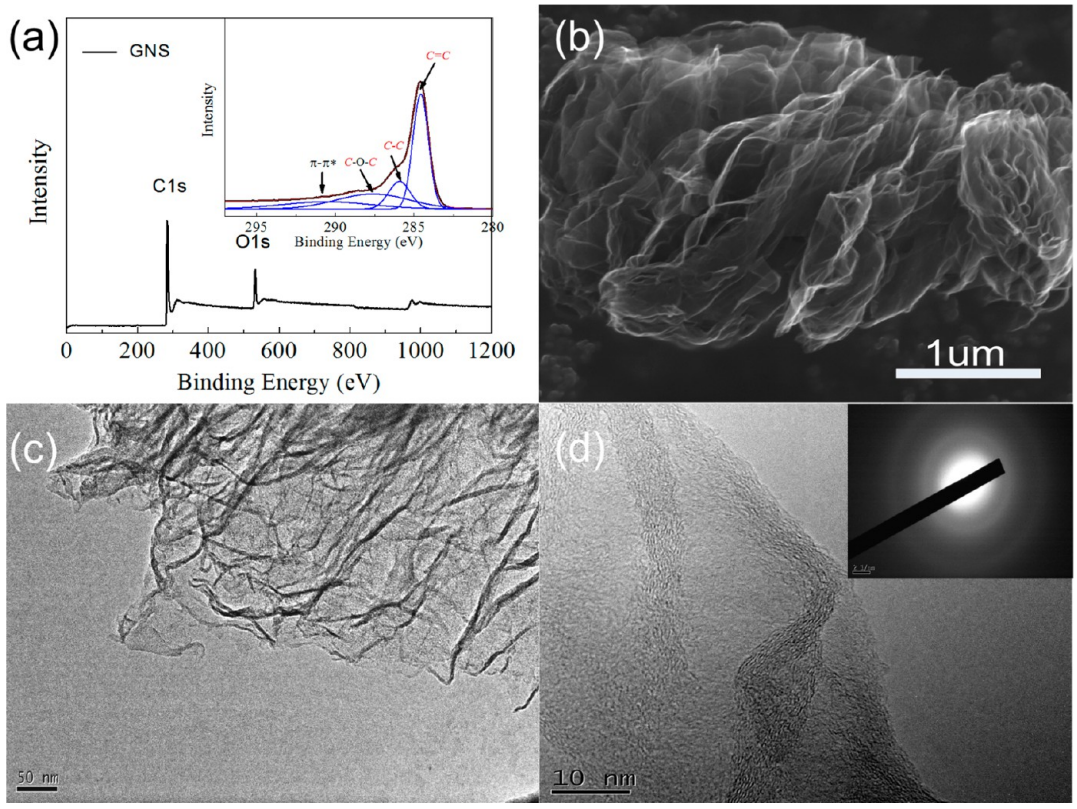

Figure 2. (a) XPS general spectra and high-resolution C 1s spectra of GNS (graphene nanoshifts), (b) SEM image of GNS, (c) TEM image of GNS, and (d) high-magnification TEM image of GNS. The inset in panel d is the SAED pattern of GNS.

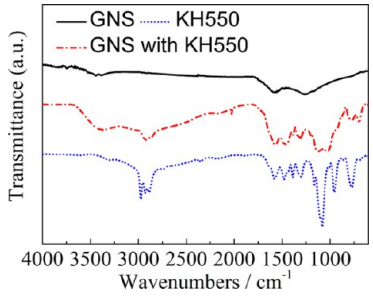

Figure 3. FTIR spectra of GNS, KH550, and KH550-modified GNS.

enhancement of I_D/I_G (about 0.87) is observed in physically blended P(VDF-TrFE-CTFE)/GNS composites. The average size of the order of the graphitic region, calculated from the empirical Tuinstra–Koenig relation,[39] is reduced from 5.1 nm for neat GNS to 4.6 nm for the P(VDF-TrFE-DB)/GNS composite. Compared with physically blended P(VDF-TrFE-CTFE)/GNS composites, chemical crosslinking of P(VDF-TrFE-DB) initiated with BPO is responsible for the significantly improved disorder of the graphene crystal and the reduced crystal size of the graphitic regions in the P(VDF-TrFE-DB)/GNS composite. The most plausible reason for this is the covalent bonds generated in the GNS of the P(VDF-TrFE-DB)/GNS composite during the free-radical-involved crosslinking of the matrix, which is in agreement with the elevated D/G ratio obtained in the chemically functionalized graphene sheets in previous reports.[41,42] The XPS spectra of 4% GNS composites are presented and assigned as shown in Figure 4b–d. Compared to GNS, F 1s and F KLL from the polymer matrix were detected in the composites, as shown in Figure 4b. The trace peaks at about 100, 150, and 400 eV assigned to Si 2p, Si 2s, and N 1s are from KH550 (γ-aminopropyl triethoxysilane).[35] The C 1s peaks of the two composites are shown Figure 4c,d. The components have been attributed to the *C*═*C* (284.6 eV), *C*–*Cl*–CF_2–CH_2– (285.6 eV), *C*–O–*C* (287.5 eV, epoxy), –*C*FH– (288.9 eV), and –CF_2–CH_2– (290.6 eV) groups for the blended composite bearing 4% GNS.[32−35] Compared to the 4% P(VDF-TrFE-CTFE)/GNS composites, two more components in the crosslinked 4% P(VDF-TrFE-DB)/GNS corresponding to CF_2 of $_{-CF_2-\overset{|}{C}F-}$ (291.0 eV) and –CF_2–*C*F_2– (292.0 eV) were observed. The component –*C*F_2–*C*F_2– (292.0 eV) is from the original main chain of the copolymer. The CF_2 on the $_{-CF_2-\overset{|}{C}F-}$ structure with low content is from the crosslinking of –CF_2–CF═CH–CF_2– of P(VDF-TrFE-DB). Meanwhile, the slight shifting in the binding energy from 285.6 to 285.9 eV of *C*–*Cl*–CF_2–CH_2– may also be attributed to the formation of the $_{-CF_2-\overset{|}{C}F-}$ structure in 4% P(VDF-TrFE-DB)/GNS composites, which is from the crosslinking of –CF_2–CF═CH–CF_2– on the main chain as well. All of the information suggests that the double bonds (–CF═CH–) are involved in the crosslinking in the composites.

To illustrate further the unusual phenomena, the DSC of two composites bearing the same 4 vol % GNS as fillers but P(VDF-TrFE-CTFE) and P(VDF-TrFE-DB) as polymeric matrix were compared side-by-side, as shown in Figure 5. As shown in Figure 5a, the crystalline behavior of P(VDF-TrFE-DB) in the composites has been significantly interfered with by the addition of GNS with only 4 vol %, including the shifting of the Curie temperature to a higher temperature, the greatly depressed melting temperature, and the overall crystallinity. However, the introduction of GNS with 4 vol % leads to no

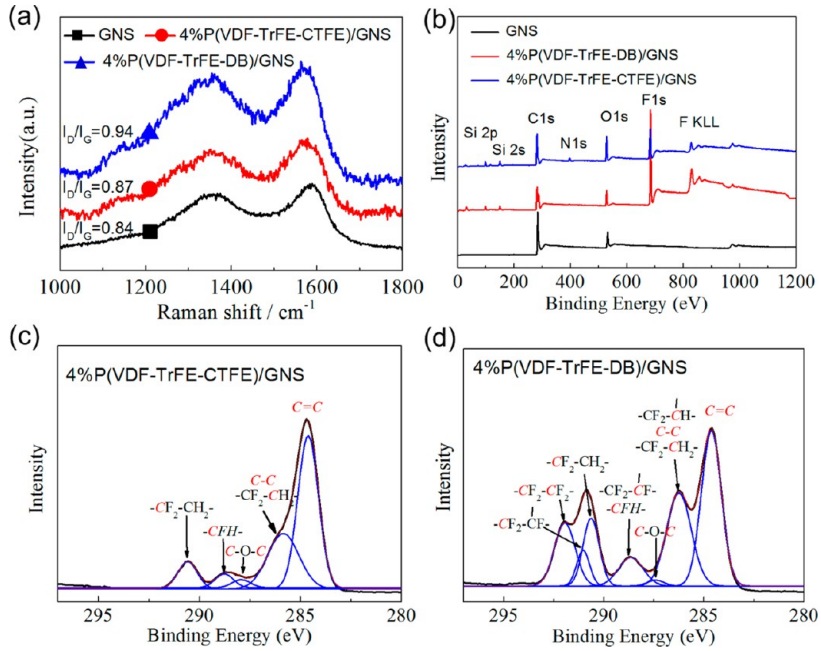

Figure 4. (a) Raman scattering and (b–d) XPS spectra of GNS, nanocomposites of P(VDF-TrFE-CTFE)/GNS, and P(VDF-TrFE-DB)/GNS with 4% GNS loaded.

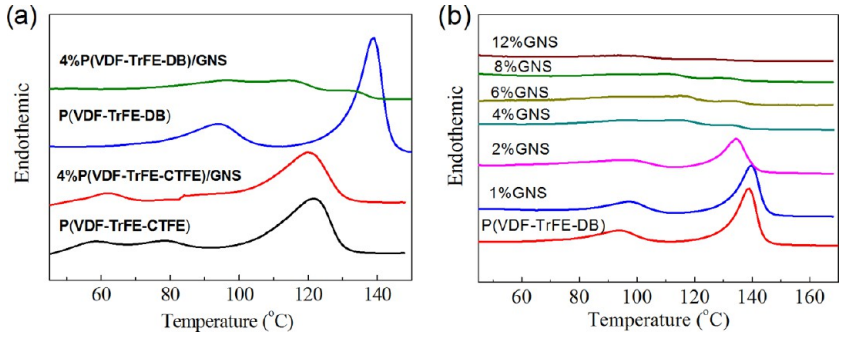

Figure 5. (a) DSC thermograms of nanocomposites of P(VDF-TrFE-CTFE)/GNS and P(VDF-TrFE-DB)/GNS. (b) DSC thermograms of P(VDF-TrFE-DB) and nanocomposites of P(VDF-TrFE-DB)/GNS. The heating rate is 10 °C/min.

visible variation of the crystalline properties of P(VDF-TrFE-CTFE), indicating that the addition of GNS exhibits little influence on the crystallization process of P(VDF-TrFE-CTFE). Although the chemical crosslinking of P(VDF-TrFE-DB) matrix initiated with BPO is expected to result in the depressed crystalline properties of the polymer matrix, the dependence of the crystalline properties on the GNS content, as indicated in Figure 5b, strongly suggests that GNS filler is affecting the crystallization of P(VDF-TrFE-DB) in the composites as well. As shown in Figure 5b, a single melting point is observed in the crosslinked P(VDF-TrFE-DB) copolymer at 139 °C, corresponding to the β-phase of P(VDF-TrFE), as was discussed in our previous study.[43] As the GNS content increases, the melting temperature is decreased from about 139 to 130 °C, and the crystallinity is reduced correspondingly. However, the crystallinity of the composites decreases greatly when more than 4 vol % GNS is introduced. This could be attributed to the impediments of the GNS introduced on the ferroelectric crystal domain nucleation and growth for its good miscibility with PVDF main chains. Meanwhile, the chemical bonds formed between P(VDF-TrFE-DB) and GNS as discussed above may be the most plausible reason for the depressed crystalline properties of the P(VDF-TrFE-DB) matrix because the high steric bulk of GNS bonded to the polymer chain may interfere with the nucleation and growth of the crystal grains.

It has been established from our previous work that BPO could effectively initiate the crosslinking of P(VDF-TrFE-DB) via a free-radical addition reaction.[31] However, some groups also reported that the free-radical addition reaction to the double bonds on GNS may also be initiated during the free-radical polymerization of the vinyl monomers, which has been utilized for the surface modification of GNS.[32,44,45] Therefore, we believe that the free-radical addition reaction can happen between P(VDF-TrFE-DB) and GNS in P(VDF-TrFE-DB)/GNS, as indicated in Scheme 1, which is responsible for the greatly improved disorder of the graphene crystal, the reduced crystal size of the graphitic regions, and the depressed crystalline properties of the P(VDF-TrFE-DB) matrix.

Besides the crystal and amorphous phase, another phase transition in P(VDF-TrFE), known as the ferro-to-paraelectric (F–P or Curie) transition relating to the mobility of highly polar β-phase crystal domains, has been widely investigated as well. At the Curie temperature, the competition between the

dx.doi.org/10.1021/am401784p | ACS Appl. Mater. Interfaces 2013, 5, 9411–9420

Scheme 1. Mechanism of the Crosslinked Reaction in P(VDF-TrFE-DB)/GNS Crosslinked Composites

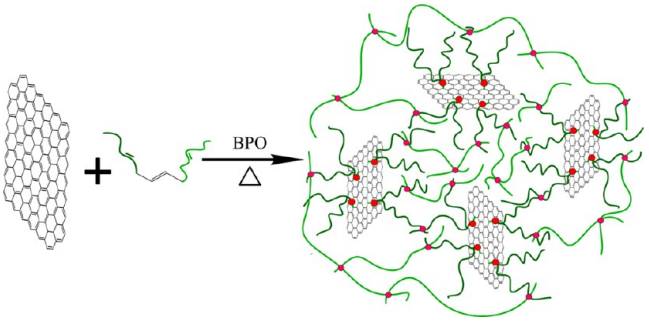

spontaneous polarization and random thermal motion of polar crystals could reach a dynamic equilibrium.[46,47] The F−P transition temperature of P(VDF-TrFE) could be tuned by varying the coupling force between the crystal domains physically (such as electron-beam irradiation) or chemically (such as incorporating another bulky monomer).[3,48] As shown in Figure 5b, the introduction of GNS in P(VDF-TrFE-DB) leads to the shifting of the Curie point to a higher temperature (from 82 to 90 °C) and the quick reduction of the transition enthalpy, whereas GNS in P(VDF-TrFE-CTFE) shows little influence on the F−P transition behavior of P(VDF-TrFE-CTFE). As discussed above, the chemical bonds between P(VDF-TrFE-DB) and GNS may hinder the switching of the polar crystal domains and result in an improved energy barrier for the F−P transition for polar crystal domains as a result of the high steric bulk of GNS bonded to the polymer chain. In other words, the so-called "domain wall" would be strengthened and stabilized. Meanwhile, the reduced crystallinity and crystal domain size of P(VDF-TrFE) are responsible for the lowered spontaneous polarization and overall heat enthalpy in the phase transition as well.

The chemical bonding between P(VDF-TrFE-DB) and GNS could also be indirectly confirmed by comparing the morphology of P(VDF-TrFE-DB)/GNS with P(VDF-TrFE-CTFE)/GNS composites, as shown in Figure 6, which shows the SEM image of 4 vol % P(VDF-TrFE-DB)/GNS and 4 vol % P(VDF-TrFE-CTFE)/GNS composites. The major difference between the composites is that the polymer matrix in P(VDF-TrFE-DB)/GNS is expected to be crosslinked with BPO as an initiator, whereas P(VDF-TrFE-CTFE) is simply blended with GNS. As shown in Figure 6a, graphitelike layer structured GNS aggregations were observed in the cross section of the 4 vol % P(VDF-TrFE-CTFE)/GNS composite. However, no visible layer structure of GNS in 4 vol % P(VDF-TrFE-DB)/GNS could be observed in Figure 6b that was similar to that in P(VDF-TrFE-CTFE)/GNS, suggesting a better compatibility of GNS with P(VDF-TrFE-DB) than P(VDF-TrFE-CTFE) because of the chemical bonding. To illustrate the results further, the panorama of the cross section of the crosslinked composites containing 4 and 6% GNS is shown in Figure 6c,d. GNSs in the films were well-distributed along the thickness direction in both composites, and some GNS could be found at the surfaces of both of the films. Compared to the composite with 4% GNS, more and larger

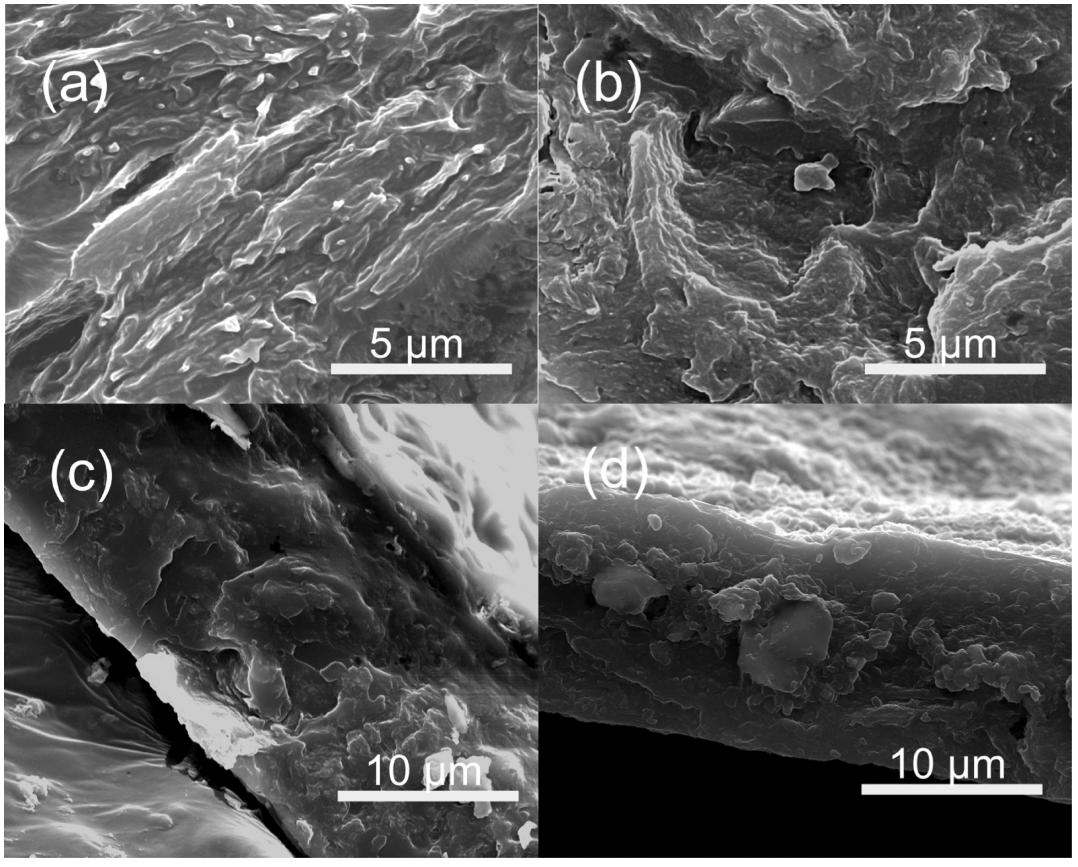

Figure 6. SEM image of the cross section of three nanocomposites. (a) 4% P(VDF-TrFE-CTFE)/GNS, (b, c) 4% P(VDF-TrFE-DB)/GNS, and (d) 6% P(VDF-TrFE-DB)/GNS.

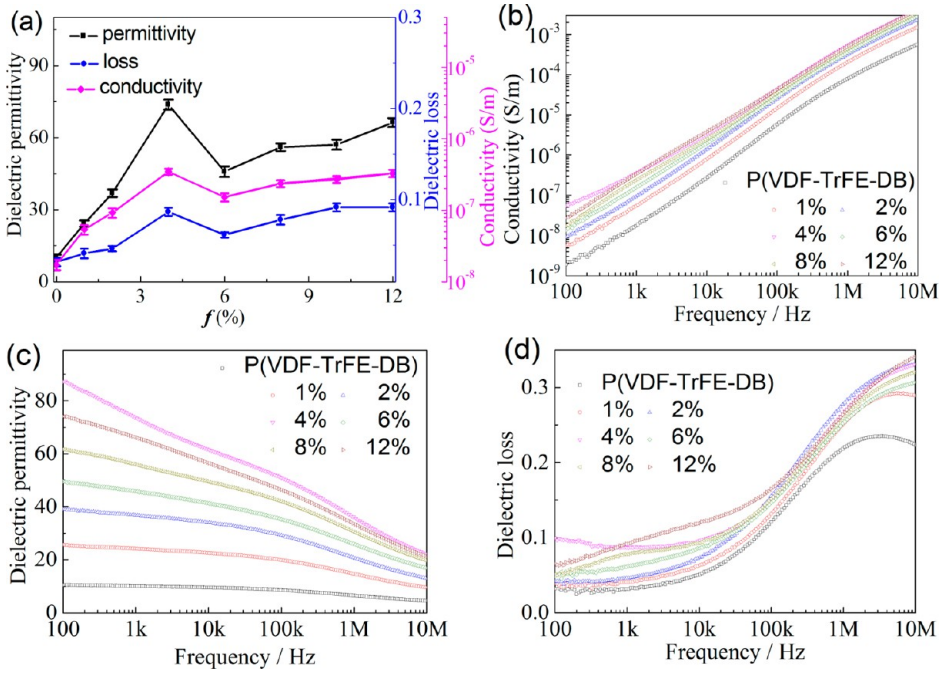

Figure 7. (a) Conductivity, dielectric permittivity, and loss of nanocomposites of P(VDF-TrFE-DB)/GNS crosslinked as a function of GNS contents at 1 kHz. (b) Conductivity, (c) dielectric permittivity, and (d) loss of nanocomposites of P(VDF-TrFE-DB)/GNS crosslinked with varied GNS content as a function of frequency.

pores were formed in the sample with 6% GNS, which has been well-addressed in the filler/polymer composites systems elevated content.[49,50]

3.3. Dielectric Properties of the P(VDF-TrFE-DB)/GNS Composites with Different GNS Content. As measured on a HP4294A LCR meter at 1 kHz, ε_r, tan δ, and the conductivity of neat P(VDF-TrFE-DB) and P(VDF-TrFE-DB)/GNS composites are presented in Figure 7a. It was found that the content of the conductive fillers of the composites played a crucial role on ε_r because their compositions are consistent. Typically, the conductivity of the composites increases as the conductive fillers content increases, which leads to the increase of dielectric permittivity and the dielectric loss of the composites.[20−22,51,52] At the threshold composition, ε_r is abruptly increased together with the large variation in both tan δ and conductivity. As the GNS content increases to 12 vol %, ε_r, tan δ, and the conductivity of the P(VDF-TrFE-DB)/GNS composites increase continuously as a function of the GNS content (f), going from 12, 0.03, and 1.73×10^{-8} S/m to 62, 0.09, and 3.29×10^{-7} S/m, respectively. Notably, an unusual enhancement is observed at f = 4 vol %, and the maximum ε_r, tan δ, and conductivity are obtained as 74, 0.08, and 3.47×10^{-7} S/m. The improved ε_r may be attributed to the Maxwell−Wagner−Sillars (MWS) effect in this type of composite, which has been discussed previously.[9,22−25] Known as interfacial polarization, MWS polarization occurs whenever there is an accumulation of charge carriers at an interface between two kinds of materials. In the present composites, the charges in conductive GNS are easily delocalized, which is driven by the applied electric field, and they accumulate at the interface of the GNS and P(VDF-TrFE) insulator layer, which contribute a large polarization. As the GNS content increases, MWS polarization is significantly improved. As a result, the dielectric permittivity of the resultant composites is enhanced quickly, which is quite normal in conductive fillers-filled composites.

Most interestingly, the typical low percolation threshold (1 to 2 wt %) usually observed in GNS-based polymeric composite systems characterized with significantly improved permittivity, large dielectric loss, and high leakage current has not been observed in the current composites even when GNS as high as 12 vol % is loaded. However, when the content of GNS is about 6 vol %, the conductivity decreased slightly, and the variation of the dielectric permittivity and loss exhibited a similar tendency as that shown in Figure 7a. This phenomenon can also be explained by the well-known increase of the pores in the composites, which restricts the electron transfer between GNS fillers.[49,50] At lower GNS content, the conductivity of the composite is low because the GNS could hardly connect with each other to form a conductive route. As GNS content increases, the adjacent GNS pieces start to contact with each other and form a conductive route on a small scale in the composites. This leads to the rapid increase of the conductivity in the composites with less than 4 vol % GNS. Meanwhile, more pores would be formed in the composites as the GNS content increases, as indicated in Figure 6c,d, which shows the negative influence on the electric properties of the composites. As a result, the conductivity together with the dielectric properties drops from 4 vol % GNS composite to 6 vol % GNS composite. However, as the GNS conductive routes increase both in amount and scale, the conductivity is more dominated by how many conductive routes are formed, and the negative effect of the pores is weakened. This leads to the increasing conductivity of composites bearing 6 to 12 vol % GNS because more conductive routes would be formed between GNS. When GNS content is sufficiently high to form the conductive route across the thickness scale, huge conductivity and dielectric properties would be observed and the GNS content is well-known as the threshold value. Over the threshold filler-loading content, the composites lose the insulating properties quickly and turn into semi- or even conductors. Fortunately, no

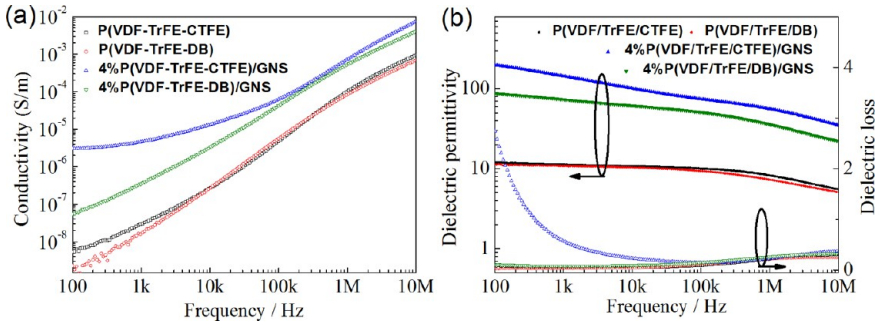

Figure 8. (a) Conductivity and (b) dielectric permittivity and loss of nanocomposites of P(VDF-TrFE-CTFE)/GNS and P(VDF-TrFE-DB)/GNS as a function of frequency. For comparison, P(VDF-TrFE-CTFE) and P(VDF-TrFE-DB) crosslinked are also shown.

percolation threshold has been observed in P(VDF-TrFE-DB)/GNS composites with up to 12 vol % GNS loading.

The dielectric and conductive properties of composites were measured under an ac electric field as a function of frequency, as indicated in Figure 7b–d. All of the composites possess a similar changing tendency in their dielectric and conductive properties against the testing frequency as that of the neat P(VDF-TrFE-DB) copolymer. All of the curves are enhanced nearly in parallel to that of the neat P(VDF-TrFE-DB) copolymer as GNS content increases except for that of f = 4 vol %. As presented in Figure 7b, the ac electrical conductivity by logarithm of the P(VDF-TrFE-DB)/GNS composites was found to increase linearly as the frequency by logarithm increases from 100 Hz to 10 MHz and was found to be slightly higher than that of P(VDF-TrFE-DB) over the whole frequency range, indicating the good insulating properties of the composites.[52] The relatively low conductivity of P(VDF-TrFE-DB)/GNS is mainly induced by two effects. First, GNS crosslinked with the double bond of P(VDF-TrFE-DB) would reduce the electron density of the conjugated network of aromatic groups in GNS as shown in Scheme 1 and thus reduces the conductivity of GNS. As a result, the effective aspect ratio of GNS is reduced and a much higher GNS content is required to form a conductive route on the whole thickness scale to reach the percolation threshold. Second, chemically bonded GNS to P(VDF-TrFE-DB) could easily be enwrapped by insulating polymer shells, leading to homogeneous dispersion, which prevents GNS from directly contacting each other, as shown in Figure 6b–d. Apparently, the ε_r value of the composites with less than 4 vol % GNS decreases slowly under the electric field below 100 kHz and drops quickly when the frequency is over 100 kHz, which is mainly induced by the semicrystalline structure of the P(VDF-TrFE-DB) matrix. The dielectric response of semicrystalline PVDF-based fluoropolymers at a frequency below 100 kHz is attributed to both the dipoles alignment in the amorphous phase in the rubber state and the weak swing of dipoles in the microcrystal grains. As the frequency increases, the contribution of the crystal phase is weakened. When the frequency is over 100 kHz, the relaxation peak was proposed to have only two random molecular motions, including the micro-Brownian motion of the noncrystalline chain segments (β-relaxation) and the molecular motion onto the amorphous/crystalline interfaces.[53,54] When the GNS loading content is over 4 vol %, the polymer matrix in the composites is mostly in the amorphous phase, and the dielectric permittivity decreases linearly as the frequency increases. Of particular interest is that all composites show a relatively low loss as well as low ac conductivity and that both are slightly higher than that of pure P(VDF-TrFE-DB) over a wide range of frequencies (100 Hz to 10 MHz), as shown in Figure 7b,d. This means that the insulating properties of the composites are well maintained even when up to 12 vol % GNS is introduced. The linear dependency of the log(conductivity) on the log(frequency) from 100 Hz to 10 MHz in the composites bearing 12 vol % GNS strongly indicates that the percolation threshold of P(VDF-TrFE-DB)/GNS composites is even higher than 12 vol % according to the percolation threshold power law.[21] It has been well-addressed that the log(conductivity) will be rather high and lose its linear dependency on the log(frequency) within a low-frequency range when the filler's content is enhanced to over the percolation threshold. However, the threshold of physically blended GNS composites is observed to be about 2 vol %.[20−26] This strongly indicates that the chemical bonding between P(VDF-TrFE-DB) and GNS could significantly enhance the threshold of the composites by reducing the aspect ratio of GNS, which is particularly important for preparing composites with consistent dielectric properties.

3.4. Dielectric Properties of 4 vol % GNS Composites Films. Apparently, the changing tendency of the dielectric and conductive properties of P(VDF-TrFE-DB)/GNS composites as a function of GNS content is inconsistent with the results reported in most of the literature in which a low threshold is reached and the dielectric loss and conductivity are greatly increased against the GNS loading contents.[20−28,51] To illustrate the unusual phenomena more clearly, ε_r, tan δ, and the conductivity of crosslinked P(VDF-TrFE-DB)/GNS and blended P(VDF-TrFE-CTFE)/GNS composites with 4 vol % GNS as a function of frequency were compared side-by-side from 100 Hz to 10 MHz at room temperature, as shown in Figure 8. The dielectric and conductive properties of the two polymer matrixes are rather close, whereas the dielectric and conductive properties of the two composites are rather different. As discussed above, all of the dielectric loss and conductive properties of P(VDF-TrFE-DB)/GNS are well-maintained and are slightly higher than its matrix. However, P(VDF-TrFE-CTFE)/GNS with 4 vol % GNS loaded lose the insulating properties and are characterized by a significantly improved conductivity and dielectric loss at low frequency, although its dielectric permittivity is slightly higher than P(VDF-TrFE-DB)/GNS.

The ac conductivity of P(VDF-TrFE-CTFE)/GNS was much higher and almost independent of frequency within a low-frequency range, indicating that the percolation threshold of blended composites was lower than 4%.[21] For instance, the conductivity of P(VDF-TrFE-CTFE)/GNS at 100 Hz was

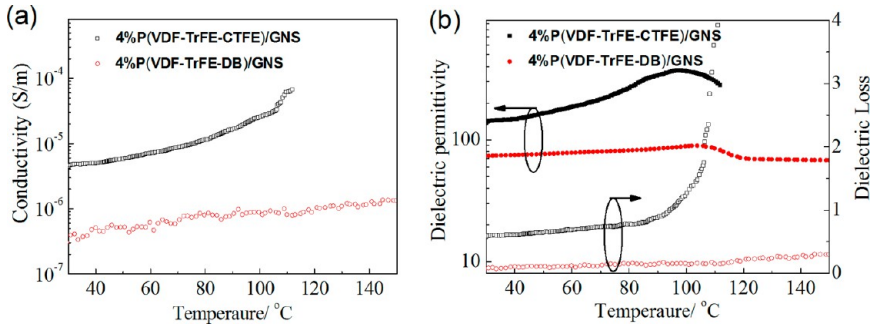

Figure 9. (a) Conductivity and (b) dielectric permittivity and loss of nanocomposites of P(VDF-TrFE-CTFE)/GNS and P(VDF-TrFE-DB)/GNS crosslinked as a function of temperature at 1 kHz.

more than 3.04×10^{-6} S/m, which is 54 times higher than that of P(VDF-TrFE-DB)/GNS with the same GNS content (5.51×10^{-8} S/m). Notably, the dielectric loss of P(VDF-TrFE-CTFE)/GNS at 100 Hz was found to be 2.74, which is about 25 times higher than that of P(VDF-TrFE-DB)/GNS (0.11), whereas ε_r of P(VDF-TrFE-CTFE)/GNS at 100 Hz reached 199, which is only 1.3 times higher than that of P(VDF-TrFE-DB)/GNS (87). The high dielectric loss in the physically blended composites could be mainly attributed to the conduction loss arising from high leakage current caused by the direct connection between the conductive fillers based on percolation threshold theory.[55] However, the chemical bonding constructed between the matrix and fillers in P(VDF-TrFE-DB)/GNS composites could significantly decrease the aspect ratio of GNS and enhance the threshold value as well as the compatibility between the matrix and GNS. As a result of these effects, the high dielectric loss caused by high conduction and the interface effect could be effectively restricted by the chemical bonding.

The chemical crosslinking of P(VDF-TrFE-DB) and GNS also leads to excellent insulating and dielectric properties of P(VDF-TrFE-DB)/GNS composites over a wide temperature range, as shown in Figure 9, where the temperature dependence of the conductivity, dielectric permittivity, and loss of P(VDF-TrFE-DB)/GNS and P(VDF-TrFE-CTFE)/GNS composites at 4 vol % GNS measured at 1 kHz is compared. The conductive and dielectric properties of P(VDF-TrFE-CTFE)/GNS are improved continuously, with a peak at the Curie temperature of P(VDF-TrFE-CTFE), and the insulating and dielectric properties are quickly lost at its melting temperature, which coincides very well with the P(VDF-TrFE-CTFE) matrix. Interestingly, the excellent insulating (conductivity from 3.1×10^{-7} to 1.3×10^{-6} S/m) and dielectric properties (ε_r from 72 to 88 and tan δ from 0.072 to 0.16) of P(VDF-TrFE-DB)/GNS are well-maintained, even at a temperature (150 °C) higher than its melting temperature (about 140 °C). The weak change of dielectric permittivity of 4 vol % P(VDF-TrFE-DB)/GNS composites at 110 °C is attributed to the F−P transition of crystalline P(VDF-TrFE) in small portion. The peak is rather small compared to the blended composites with a much higher crystallinity and larger peak at this temperature. This could be attributed to the excellent mechanical properties that maintain the capability of the 3D crosslinked structure formed by the crosslinked P(VDF-TrFE-DB) matrix, as shown in Scheme 1, which may restrict the mobility of the polymer chains at the temperature above its melting temperature and reduce the conductivity and loss induced. This also means that P(VDF-TrFE-DB)/GNS composites are allowed to be utilized at high temperatures without the concern of losing their mechanical properties. The significantly increased dielectric permittivity and decreased dielectric loss and conductivity achieved in the P(VDF-TrFE-DB)/GNS composites strongly suggest that improving the compatibility by chemically crosslinking the polymer matrix with GNS filler could be a facile and promising method to fabricate high dielectric composites with excellent performance.

4. CONCLUSIONS

We prepared a series of P(VDF-TrFE)/GNS high dielectric nanocomposites via facilely blending KH550 surface-modified GNS with double bonds containing P(VDF-TrFE) in solution. After initiation, the 3D crosslinked structure between the P(VDF-TrFE) matrix and GNS is constructed because of the free-radical addition reactions between them. The chemical crosslinking on GNS leads to the reduction of its effective aspect ratio and its depressed dielectric and conductive properties as well as its improved compatibility with the P(VDF-TrFE) matrix. The reduced conductivity of GNS and the inhibited MWS effects between the GNS and P(VDF-TrFE) interface induced by the crosslinking are responsible for the well-maintained low dielectric loss and conductivity as well as the significantly improved dielectric constant in the P(VDF-TrFE-DB)/GNS composites with a high GNS loading content over a wide range of frequencies and temperatures. Considering the excellent thermal stability, mechanical, dielectric, and insulating properties of the P(VDF-TrFE-DB)/GNS composites, establishing chemical crosslinks between a polymer matrix and fillers in situ as presented in this work may open a facile route toward fabricating high-performance nanocomposites by inhibiting the poor compatibility between the fillers and polymeric matrix.

AUTHOR INFORMATION

Corresponding Author

*Tel: 86-29-82668546. E-mail: zhichengzhang@mail.xjtu.edu.cn.

Notes

The authors declare no competing financial interest.

ACKNOWLEDGMENTS

This work was financially supported by the National Basic Research Program of China (973 Program; grant no.2009CB623306), International Science & Technology Cooperation Program of China (grant nos. 2010DFR50480 and 2013DFR50470), National Nature Science Foundation of China-NSAF (grant nos. 10976022, 50872107, 50903065, and

51103115), Natural Science Basic Research Plan in Shaanxi Province of China (grant no. 2013JZ003), and Program for New Century Excellent Talents in University, and Fundamental Research Funds for the Central Universities.

REFERENCES

(1) Kawai, H. *Jpn. J. Appl. Phys.* **1969**, *8*, 975−976.
(2) Zhang, Q. M.; Li, H. F.; Poh, M.; Xia, F.; Cheng, Z. Y.; Xu, H. S.; Huang, C. *Nature* **2002**, *419*, 284−287.
(3) Zhang, Q. M.; Bharti, V.; Zhao, X. *Science* **1998**, *280*, 2101−2104.
(4) Naber, R. C. G.; Tanase, C.; Blom, P. W. M.; Gelinck, G. H.; Marsman, A. W.; Touwslager, F. J.; Setayesh, S.; Leeuw, D. M. *Nat. Mater.* **2005**, *4*, 243−248.
(5) Kang, S. J.; Park, Y. J.; Hwang, J.; Jeong, H. J.; Lee, J. S.; Kim, K. J.; Kim, H. C.; Huh, J.; Park, C. *Adv. Mater.* **2007**, *19*, 581−586.
(6) Chu, B. J.; Zhou, X.; Ren, K. L.; Neese, B.; Lin, M. R.; Wang, Q.; Bauer, F.; Zhang, Q. M. *Science* **2006**, *313*, 334−336.
(7) Dang, Z. M.; Lin, Y. H.; Nan, C.W. *Adv. Mater.* **2003**, *15*, 1625−1629.
(8) Shen, Y.; Lin, Y. H.; Li, M.; Nan, C. W. *Adv. Mater.* **2007**, *19*, 1418−1422.
(9) Dang, Z. M.; Wang, L.; Yin, Y.; Zhang, Q.; Lei, Q. Q. *Adv. Mater.* **2007**, *19*, 852−857.
(10) Wang, L.; Dang, Z. M. *Appl. Phys. Lett.* **2005**, *87*, 042903-1−042903-3.
(11) Dang, Z. M.; Yuan, J. K.; Zha, J. W.; Zhou, T.; Li, S. T.; Hu, G. H. *Prog. Mater. Sci.* **2012**, *57*, 660−723.
(12) Nan, C. W. *Prog. Mater. Sci.* **1993**, *37*, 1−116.
(13) Zhu, Y. W.; Murali, S.; Cai, W. W.; Li, X. S.; Suk, J. W.; Potts, J. R.; Ruoff, R. S. *Adv. Mater.* **2010**, *22*, 3906−3924.
(14) Stankovich, S.; Dikin, D. A.; Dommett, G. H. B.; Kohlhaas, K. M.; Zimney, E. J.; Stach, E. A.; Piner, R. D.; Nguyen, S. T.; Ruoff, R. S. *Nature* **2006**, *442*, 282−286.
(15) Kim, H.; Abdala, A. A.; Macosko, C. W. *Macromolecules* **2010**, *43*, 6515−6530.
(16) Kuilla, T.; Bhadra, S.; Yao, D.; Kim, N. H.; Bose, S.; Lee, J. H. *Prog. Polym. Sci.* **2010**, *35*, 1350−1375.
(17) Li, B.; Zhong, W. H. *J. Mater. Sci.* **2011**, *46*, 5595−5614.
(18) Sengupta, R.; Bhattacharya, M.; Bandyopadhyay, S.; Bhowmick, A. K. A *Prog. Polym. Sci.* **2011**, *36*, 638−670.
(19) Singh, V.; Joung, D.; Zhai, L.; Das, S.; Khondaker, S. I.; Seal, S. *Prog. Mater.Sci.* **2011**, *56*, 1178−1271.
(20) Tang, H.; Ehlert, G. J.; Lin, Y.; Sodano, H. A. *Nano Lett.* **2012**, *12*, 84−90.
(21) He, F.; Lau, S.; Chan, H. L.; Fan, J. *Adv. Mater.* **2009**, *21*, 710−715.
(22) Javada, A.; Xiao, Y.; Xu, W.; Gong, S. *J. Mater. Chem.* **2012**, *22*, 830−834.
(23) Wang, D.; Bao, Y.; Zha, J. W.; Zhao, J.; Dang, Z. M.; Hu, G. H. *ACS Appl. Mater. Interfaces* **2012**, *4*, 6273−6279.
(24) Cui, L.; Lu, X.; Chao, D.; Liu, H.; Li, Y.; Wang, C. *Phys. Status Solidi A* **2011**, *208*, 459−461.
(25) Shang, J.; Zhang, Y.; Li, Y.; Shen, B.; Lv, F.; Chu, P. K. *Mater. Chem. Phys.* **2012**, *134*, 867−874.
(26) Fan, P.; Wang, L.; Yang, J.; Chen, F.; Zhong, M. *Nanotechnology* **2012**, *23*, 365702.
(27) Yu, J.; Huang, X.; Wu, C.; Jiang, P. *IEEE Trans. Dielectr. Electr. Insul.* **2011**, *18*, 478−484.
(28) Shang, J.; Zhang, Y.; Yu, L.; Luan, X.; Shen, B.; Zhang, Z.; Lv, F.; Chu, P. K. *J. Mater. Chem. A* **2013**, *1*, 884−890.
(29) Pan, D.; Wang, S.; Zhao, B.; Wu, M.; Zhang, H.; Wang, Y.; Jiao, Z. *Chem. Mater.* **2009**, *21*, 3136−3142.
(30) Zhang, Z. C.; Meng, Q. J.; Chung, T. C. M. *Polymer* **2009**, *50*, 707−715.
(31) Tan, S. B.; Li, J.; Gao, G.; Li, H.; Zhang, Z. C. *J. Mater. Chem.* **2012**, *22*, 18496−18504.
(32) Hsiao, M. C.; Liao, S. H.; Yen, M. Y.; Liu, P. I.; Pu, N. W.; Wang, C. A.; Ma, C. C. M. *ACS Appl. Mater. Interfaces* **2010**, *2*, 3092−3099.
(33) Dubin, S.; Gilje, S.; Wang, K.; Tung, V. C.; Cha, K.; Hall, A. S.; Farrar, J.; Varshneya, R.; Yang, Y.; Kaner, R. B. *ACS Nano* **2010**, *4*, 3845−3852.
(34) Stankovich, S.; Dikin, D. A.; Piner, R. D.; Kohlhaas, K. A.; Kleinhammes, A.; Jia, Y.; Wu, Y.; Nguyen, S. T.; Ruoff, R. S. *Carbon* **2007**, *45*, 1558−1565.
(35) Xu, F. J.; Song, Y.; Cheng, Z. P.; Zhu, X. L.; Zhu, C. X.; Kang, E. T.; Neoh, K. G. *Macromolecules* **2005**, *38*, 6254−6258.
(36) Acik, M.; Mattevi, C.; Gong, C.; Lee, G.; Cho, K.; Chhowalla, M.; Chabal, Y. J. *ACS Nano* **2010**, *10*, 5861−5868.
(37) Acik, M.; Lee, G.; Mattevi, C.; Chhowalla, M.; Cho, K.; Chabal, Y. J. *Nat. Mater.* **2010**, *10*, 840−845.
(38) Dreyer, D. R.; Murali, S.; Zhu, Y.; Ruoff, R. S.; Bielawski, C. W. *J. Mater. Chem.* **2011**, *10*, 3443−3447.
(39) Ferrari, A.; Robertson, C. J. *Phys. Rev. B* **2000**, *61*, 14095−14107.
(40) Tuinstra, F.; Koenig, J. L. *J. Chem. Phys.* **1970**, *53*, 1126−1130.
(41) Georgakilas, V.; Bourlinos, A. B.; Zboril, R.; Steriotis, T. A.; Dallas, P.; Stubos, A. K.; Trapalis, C. *Chem. Commun.* **2010**, *46*, 1766−1768.
(42) Kudin, K. N.; Ozbas, B.; Schniepp, H. C.; Prud'homme, R. K.; Aksay, I. A.; Car, R. *Nano Lett.* **2008**, *8*, 36−41.
(43) Li, J. J.; Tan, S. B.; Ding, S. J.; Li, H. Y.; Yang, L. J.; Zhang, Z. C. *J. Mater. Chem.* **2012**, *22*, 23468−23476.
(44) Kan, L.; Xu, Z.; Gao, C. *Macromolecules* **2011**, *44*, 444−452.
(45) Shen, J.; Hu, Y.; Li, C.; Qin, C.; Ye, M. *Small* **2009**, *5*, 82−85.
(46) Tajitsu, Y.; Chiba, A. *Appl. Phys. Lett.* **1980**, *36*, 286−288.
(47) Yamada, T.; Ueda, T.; Kitayama, T. *J. Appl. Phys.* **1981**, *52*, 948−952.
(48) Chung, T. C.; Petchsuk, A. *Macromolecules* **2002**, *35*, 7678−7682.
(49) Li, K.; Wang, H.; Xiang, F.; Liu, W.; Yang, H. *Appl. Phys. Lett.* **2010**, *97*, 222905.
(50) Qi, L.; Lee, B. I.; Chen, S. H.; Samuels, W. D.; Exarhos, G. J. *Adv. Mater.* **2005**, *17*, 1777−1781.
(51) Yuan, J. K.; Yao, S. H.; Dang, Z. M.; Sylvestre, A.; Genestoux, M.; Bai, J. B. *J. Phys. Chem. C* **2011**, *115*, 5515−5521.
(52) Zhang, J.; Mine, M.; Zhu, D.; Matsuo, M. *Carbon* **2009**, *47*, 1311−1320.
(53) Guan, F. X.; Wang, J.; Pan, J. L.; Wang, Q.; Zhu, L. *Macromolecules* **2010**, *43*, 6739−6748.
(54) Hahn, B.; Wendorff, J.; Yoon, D. Y. *Macromolecules* **1985**, *18*, 718−721.
(55) Wu, C.; Huang, X.; Wang, G.; Wu, X.; Yang, K.; Li, S.; Jiang, P. *J. Mater. Chem.* **2012**, *22*, 7010−7019.